

Indentation Fracture in Brittle Rocks and Glasses

M. V. SWAIN*

B. R. LAWN†

The nature of localised cracking about indentations in Westerly granite and silicate glass is examined. Characteristic fracture patterns are identified, with distinctions between 'sharp' and 'blunt' indenters, 'loading' and 'unloading' crack driving forces, providing the basis for classification. Indentation-induced surface-removal processes in brittle solids are thence described in terms of a tensile mode of failure, in which cracks initiate and propagate within an (approximately) radially diminishing contact field. In their well-developed form the indentation cracks tend to a certain geometrical similarity, which lends itself to a simple fracture mechanics analysis. Using glass as a model material, extensive measurements of crack size as a function of indentation load are presented in support of the similarity equations. Comparative observations of crack patterns in sectioned glass and granite specimens serve to demonstrate the applicability of the analysis to brittle rocks.

INTRODUCTION

The nature of surface-removal processes in indentation-type operations on brittle rocks is poorly understood. Part of the problem is that rocks are invariably complex microstructurally, and the mechanisms by which failure modes initiate and propagate tend to vary widely. Also, rocks are opaque materials, so that one is usually restricted to 'before-and-after' studies of indentation specimens. The general approach adopted by rock-mechanics workers appears to have been one of devising some empirical failure criterion or 'efficiency parameter' for specific surface-removal events. While this approach may take us close to a characterization of events in important geological engineering situations, such as the drilling and crushing of ores, it provides little or no insight into the fundamental modes of failure themselves.

These difficulties typical of the testing of rocks are not so apparent in other, less complex brittle solids. Inorganic glasses, in particular, being transparent, isotropic and homogeneous, are ideal 'model' materials for studying basic brittle properties [1,2]. This is particularly so in indentation fracture experiments (reviewed in Ref. [3]), where the entire evolution of fracture may be followed with minimal complication *during* the testing. Such studies reveal features in near-surface failure modes which are not at all evident from mere before-and-after examinations. For instance, the cracks most effective in causing surface chipping may

actually initiate and propagate during *unloading*, rather than *loading*, of the indenter [4,5]. While it is recognised that the mechanical behaviour of brittle rocks and glasses may differ widely in many respects, striking similarities in the general indentation fracture patterns suggest a certain universality in the processes associated with surface removal.

It is the main aim of this paper to survey the state of knowledge of indentation fracture in glasses, and thence to indicate how this knowledge may be applied to the corresponding phenomenon in rocks. Basically, the approach is to characterise the geometry and extent of indentation-induced cracking in terms of the contact stress field. This leads to expressions for the scale of microfracturing in terms of the indenter load, from which the role of material properties (e.g. hardness, stiffness, toughness) and extraneous variables (e.g. indenter geometry, environment) may be (either explicitly or implicitly) inferred. Some comparative observations on commercial silicate glasses and Westerly granite serve to illustrate the essential elements of the theoretical description.

BASIC MODES OF INDENTATION FRACTURE: USE OF THE GEOMETRICAL SIMILARITY PRINCIPLE

Indentation stress fields

When the flat surface of a solid is loaded with a hard indenter, the solid experiences a complex stress field. The detailed nature of this field will depend on several factors, notably the mechanical response of the solid (linear elastic, elastic/brittle, elastic/plastic, and so on) and the geometry of the indenter (e.g. 'blunt' or

* Martin Marietta Laboratories, 1450 South Rolling Road, Baltimore, MD 21227, U.S.A.

Present address: Cavendish Laboratory, Department of Physics, University of Cambridge, Madingley Road, Cambridge, U.K.

† School of Physics, University of New South Wales, Kensington, N.S.W. 2033, Australia.

'sharp' [6]. While this multiplicity of factors rules out a comprehensive discussion of the various types of contact field, some perfectly general features may be identified in certain limiting situations. Thus, whereas ill-defined regions of stress concentration may exist in the immediate vicinity of the contact area, depending in detail on the mechanical and geometrical factors just mentioned, remote from this area, the elastic field may be adequately represented by appropriate line- (stress inversely proportional to radial distance) or point- (stress inversely proportional to square of radial distance) loading configurations (St. Venant's principle) [7]. Consequently, once the indentation fracture system reaches the stage where it may be considered 'well-developed', fine details in the nature of the contact will be of only secondary importance. Any such simplifications in the approach to a stress analysis will be lost during the unloading, where residual fields associated with incompatibility strains between irreversible deformation zone and surrounding elastic matrix inevitably come into play [5].

The stress field assumes a central position in the pre-determination of both the path and the driving force for fracture (see, for example, chapter 3, Ref. [2]). If the fracture proceeds via a truly brittle cleavage (or 'opening') mode, as is generally the case in silicate solids, it is the tensile component of the field* which is of prime concern [3]. With blunt indenters the dominant tension occurs in the near field just outside the contact area, and drops off, very rapidly at first, along a trajectory which extends downward and outward from the surface. With sharp indenters, the dominant tension tends to develop immediately below the penetrating edge or point, correspondingly diminishing along a downward-extending trajectory coincident with the loading direction. At the same time, one cannot ignore the other components of stress, notably the shear and hydrostatic components, in the indentation field; for these control the operation of the irreversible deformation modes (plastic flow, densification, crushing) responsible for the hardness impression, and thus ultimately determine (albeit indirectly) the residual stress field upon removal of the indenter.

Evolution of crack patterns

We are now in a position to understand qualitatively the evolution of the general indentation fracture pattern, as depicted schematically in Fig. 1:

(i) *Crack nucleation.* We must first ask how the cracks begin (see, for example, chapter 2, Ref. [2]). The typical brittle solid contains a profusion of pre-existing 'flaws', any one of which may provide a critical nucleus for fracture. In homogeneous materials, such as glass, such flaws must commonly arise as a result of microscopic

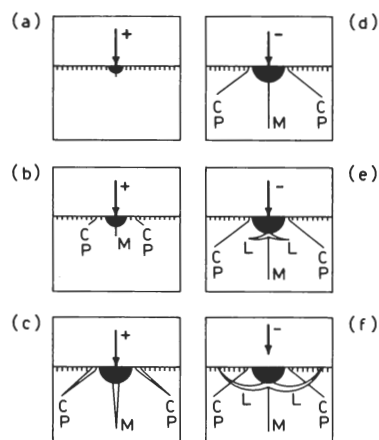


Fig. 1. Schematic of indentation-crack evolution during loading (+) and unloading (-) half-cycles. Fracture may initiate from flaws either pre-present (usually at surface) or deformation-induced (at position of maximum stress concentration, usually immediately below indenter tip). C, P denotes cone or prism crack, M denotes median crack, L denotes lateral crack.

contact damage at the surface. In inhomogeneous materials, such as rocks, the flaws correspond to microstructural defects, such as grain or interphase boundaries. Alternatively, crack nuclei may be created by deformation processes during the very act of indentation itself. The stress field considerations outlined above indicate that pre-existing, near-surface flaws will tend to dominate the crack initiation in the case of blunt indenters, and that deformation-induced flaws below the surface will likewise dominate in the case of sharp indenters. The two classes of crack nuclei are accordingly schematised in Fig. 1a.

(ii) *Crack formation.* The dominant flaw begins to extend into the solid, in a stable manner, as the indenter load is increased. This initial stage of restricted growth may be described in terms of an energy barrier to full propagation, due to the inhibiting effect of 'stress cutoffs' in the field associated with a non-zero contact area (bearing in mind that true line- or point-force loadings would produce stress singularities at the contact) [6]. Typically, the depth to which the crack must grow before overcoming the barrier is small compared with the characteristic dimension of the contact area. The presence of an appropriate hostile environment, e.g. water vapour in the case of glass fracture, can cause 'barrier tunnelling' via subcritical crack growth, thereby lowering the applied load necessary to develop fully the fracture pattern [8, 9]. Depending on the indenter geometry, as discussed in (i) above, either, sometimes both, of the two flaw types represented in Fig. 1a will form stable cracks. This is shown in Fig. 1b.

(iii) *Crack propagation.* Once the formation energy barrier is exceeded for a given crack, spontaneous, rapid propagation ensues. At a depth somewhat greater than the contact dimension, the tensile driving force falls below that necessary to maintain growth, whence the crack again becomes stable. The crack is then said to be 'well developed', in that near-contact details no longer occupy an important place in the fracture mechanics. Figure 1c depicts this stage in the growth.

*Actually, the tensile stress component reduces toward zero as the loading configuration tends from point-force to line-force type [7]. However, the tensile strain component (due to a Poisson's ratio effect) remains non-zero. The fracture can therefore always proceed according to an opening mode in the general indentation field.

The best-studied case of a well-developed indentation fracture is that of the Hertzian ‘cone’ crack, initiated from a surface flaw by the elastic contact of a normally loaded sphere [3, 6, 8, 11] (outer crack traces in Fig. 1c). Another important case is the ‘median’ half-penny crack, initiated from a deformation-induced flaw by the tip of a sharp cone or pyramid indenter [3–6] (inner crack trace in Fig. 1c). Both types expand radially outward on near-circular fronts, the axes of which pass through the loading point and lie normal and parallel to the surface for cone and median cracks respectively. Several such well-developed cracks may propagate successively or even simultaneously, under the action of further mechanical or chemical forces, in more general loading configurations.

(iv) *Unloading cracks.* Reversal of the indentation load causes the cone and median cracks to close (imperfectly) [11], Fig. 1d. More importantly, residual stresses due to mismatch at boundary between irreversibly deformed material and surrounding elastic matrix begin to impress themselves on the field, thereby creating conditions favourable to the initiation (Fig. 1e) and propagation (Fig. 1f) of an entirely new crack system. This is the system of ‘lateral’ cracks, which emanate from the deformation zone and propagate sideways and upward in a stable manner toward the specimen surface [4, 5]. Lateral cracking is not yet well understood, owing to the relatively ill-defined nature of the residual tensile field responsible for it, yet would appear to constitute the most efficient of all the indentation fracture modes as a means of surface removal. Its driving force is, however, clearly tied up with the intensity of the deformation processes, a factor strongly favoured by the enhanced stress-concentrating power of sharp indenters.

Similarity relations—loading half-cycle

It is possible to avoid most of the analytical complexities associated with the general indentation fracture problem by noting that the cracks tend, in the advanced stages of loading, to a certain geometrical similarity. Thus, for example, in the case of point-force indenters both cone and median cracks may be considered to be ‘penny-like’ (i.e. expanding on an ever-increasing circular front), while in the case of line-force indenters the counterparts of these cracks, prism or extended median cracks, may be represented as ‘through-planar’ (expanding on an infinite, linear front). This paves the way for a straightforward evaluation of the Griffith–Irwin condition for crack equilibrium (see chapter 3 of Ref. [2]), in terms of a scaling argument, to obtain basic relationships between the scale of cracking and the applied load for the positive half-cycle.

Accordingly, let us investigate the equilibrium requirements for the indentation configurations of Fig. 2. In this figure P is the applied load, acting either over a line L , i.e. $P = P_L L$, with P_L a line force per unit length, or over a point contact, and c is a characteristic crack length. We consider the balance between

the mechanical energy, U_M , and the surface energy, U_S , for a virtual displacement δc in the crack system. The appropriate surface energy change is immediately written in terms of incremental crack area,

$$\delta U_S \propto \Gamma(L\delta c) \text{ (line)} \quad (1a)$$

$$\delta U_S \propto \Gamma(c\delta c) \text{ (point)}, \quad (1b)$$

where Γ is the fracture surface energy (energy required to create unit area of new crack surface). For the mechanical energy change, we note that the stress intensity of the indentation field may be specified as the load divided by a characteristic area (taken as area of the surface everywhere distance c from the contact) supporting this load ($\sigma \propto P/Lc$, line; $\sigma \propto P/c^2$, point), that the strain energy density is determined by the stress squared divided by an appropriate elastic modulus ($\propto P^2/L^2c^2E$, line; $\propto P^2/c^4E$, point; E is Young’s modulus), and that the volume of stressed material associated with the crack extension is that traced out by the characteristic support area ($\propto Lc\delta c$, line; $\propto c^2\delta c$, point). Then we have

$$\delta U_M \propto -P^2\delta c/LcE \text{ (line)} \quad (2a)$$

$$\delta U_M \propto -P^2\delta c/c^2E \text{ (point)}. \quad (2b)$$

Here the negative sign indicates that the mechanical energy diminishes as the crack extends. The Griffith–Irwin energy-balance condition for crack equilibrium simply requires that the total energy change of the system be zero (principle of virtual work): i.e. $\delta U_S = -\delta U_M$, from which we obtain

$$c = \kappa_l P^2/2\Gamma E L^2 = \kappa_l P_L^2/2\Gamma E \text{ (line)} \quad (3a)$$

$$c = (\kappa_p P^2/2\Gamma E)^{1/3} \text{ (point)}, \quad (3b)$$

where the dimensionless κ terms are here defined in accordance with an earlier notation [6]. Toughness (Γ) and stiffness (E) are thus controlling parameters for this type of cracking.

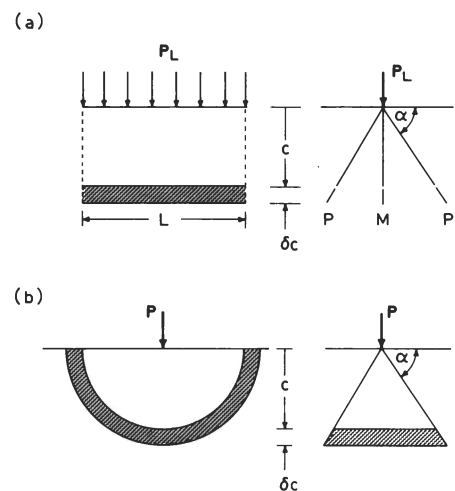


Fig. 2. Indentation–crack parameters for loading half-cycle. (a) Line-force configurations, showing side view (left) and end view (right) of median (M) and prism (P) cracks. (b) Point-force configurations, showing side view of median crack (left) and side view of cone crack (right).

More rigorous fracture mechanics analyses, while confirming the essential functional form of Eq. (3), indicate that certain angular terms, representative of contact and crack geometries, should enter via the proportionality 'constants'. These additional terms account for the fact that only a fractional component of the total applied load is effective in wedging open the cracks. The appropriate constants in Eq. (3), as calculated for smooth* contacts, are as follows [3, 4, 6]:

$$\kappa_l^s = (1 - \nu^2)/\pi \tan^2 \psi \quad (\text{line, sharp}) \quad (4a)$$

$$\kappa_l^b = \kappa_l^b(\nu, \alpha) \quad (\text{line, blunt}) \quad (4b)$$

$$\kappa_p^s = (1 - \nu^2)/\pi^3 \tan^2 \psi \quad (\text{point, sharp}) \quad (5a)$$

$$\kappa_p^b = \kappa_p^b(\nu, \alpha) \quad (\text{point, blunt}) \quad (5b)$$

where ψ is the wedging half-angle of a sharp indenter, α is the crack inclination angle (Fig. 2) in the case of blunt indenters, and ν is Poisson's ratio; the functions $\kappa^b(\nu, \alpha)$ for blunt indenters are relatively difficult to evaluate analytically, and are generally computed by numerical techniques such as finite-element analysis [12].

Similarity relations—unloading half-cycle

Let us now investigate the possibility of obtaining suitable fracture mechanics equations for the lateral cracks which form as the indenter is unloaded. We have already alluded to the uncertain nature of the residual field which provides the driving forces for these cracks. This would appear to rule out any possibility of obtaining simple relationships, analogous to those of Eq. (3), between the load level reached and the scale of the ensuing lateral cracking.

On the other hand, some progress can be made if the residual driving forces are of sufficient intensity that the lateral cracks are made to intersect the specimen surface. In this case one may reasonably hypothesize that the size of the resultant chip should scale with that of the hardness impression, for the deformation associated with this impression constitutes the *source* of the residual field. Noting that for geometrically similar indentations we may relate the characteristic dimension α of the residual impression (Fig. 3) to the peak load P^m through the standard hardness (mean contact pressure) relations,

$$H = P^m/2La \quad (\text{line}) \quad (6a)$$

$$H = P^m/\alpha\pi a^2 \quad (\text{point}), \quad (6b)$$

α being a factor determined by indenter geometry ($\alpha = 1$ for axially symmetric indenters), we may write the characteristic linear dimension c' of the lateral

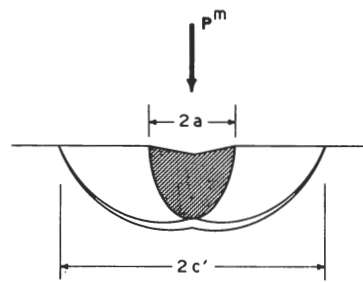


Fig. 3. Indentation-crack parameters for unloading half-cycle, showing chip-formation configuration of lateral crack system.

crack (Fig. 3) in the form

$$c' = \lambda_l a = \lambda_l P^m/2HL = \lambda_l P_L^m/2H \quad (\text{line}) \quad (7a)$$

$$c' = \lambda_p a = \lambda_p (P^m/\alpha\pi H)^{1/2} \quad (\text{point}). \quad (7b)$$

The λ terms are scaling factors, which may be expected to depend upon indenter geometry and perhaps material structure. We note that the hardness (H), rather than the toughness or stiffness, is the controlling parameter in this case.†

EXPERIMENTAL RESULTS

Procedure

Indentation tests were carried out on slabs of glass and granite under a variety of conditions. The indenters used, Fig. 4, were chosen to represent typical tool bits of rock drilling machines (e.g. 'mole' tunnel borer), and were all made from tungsten carbide. Figure 4a shows a bevelled wedge (centre), either ground to an edge (left: included half-angle $\psi = 30^\circ$ or 37.5°) or ground with a flat (right: flat half-width $\alpha = 0.75$ mm), for producing 'linear' indentations. Figure 4b similarly shows 2 axially

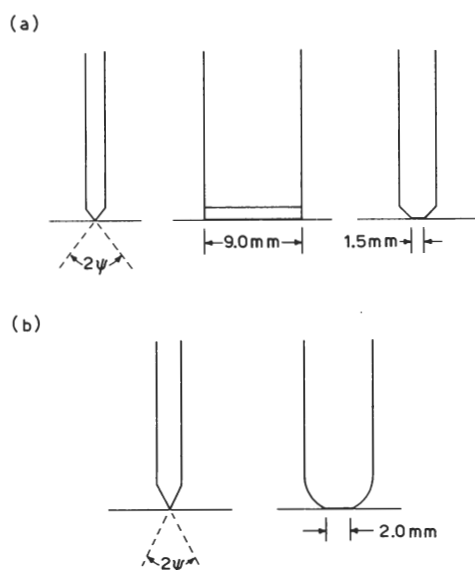


Fig. 4. Indenters used in present tests. (a) Linear indenters (planar symmetry), showing side view (centre) and end views of sharp (left) and blunt (right) wedges. (b) Point indenters (axial symmetry), showing side views of sharp (left) cone or pyramid and blunt (right) truncated hemisphere. All indenters, other than commercial Vickers diamond pyramid, of tungsten carbide. In the case of the sharp indenters the characteristic half-angle ψ was variable.

*For rough contacts the effect of friction may be incorporated by replacing ψ in Eqs. (4) and (5) by $\psi' = \psi + \arctan \mu$, μ being the coefficient of sliding friction between indenter and specimen at the contact [6]. According to this modification, friction may be seen as effectively 'blunting' the indenter tip during the loading half-cycle.

†However, it is as well to acknowledge that toughness and stiffness must play a role in determining the resistance to lateral crack propagation prior to chip formation.

symmetric indenter geometries, those of a cone (left: half-angles ranging over $\psi = 30^\circ$ to 80° in 10° intervals) and a sphere with flat (right: flat radius $\alpha = 1.0$ mm), for producing 'point' indentations. For each individual test the appropriate indenter was mounted onto the crosshead of a Universal testing machine, and thence brought to bear on the surface of the specimen. The crosshead was operated at a fixed speed of 0.5 mm min^{-1} throughout, and the load-displacement characteristic of the entire indentation event duly monitored.

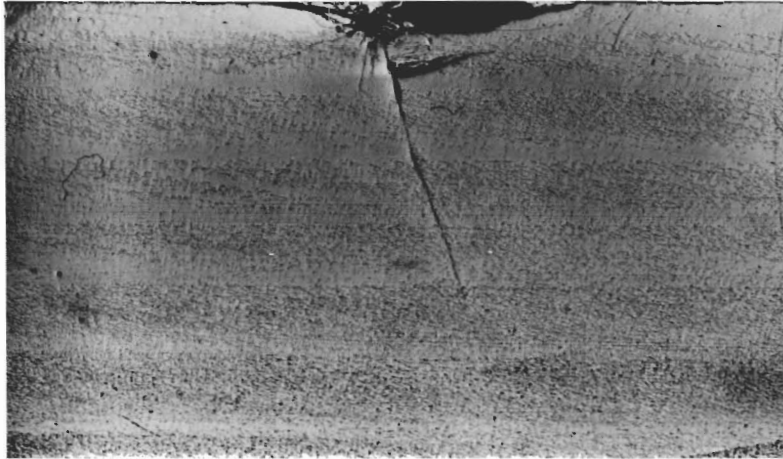
The glass specimens used were as-received slabs, 12.7 mm thick, of commercial soda-lime glass. Westerly granite slabs were cut from large rock samples, and ground flat to a thickness of 50 mm with a diamond wheel (grade 200 grit). All specimens were indented under normal laboratory environment conditions. The indentation load was always made sufficiently great that the resultant crack pattern could be considered to be 'well developed', as signified by the extensive damage features observed about the contact site.

In the glass specimens the progress of the indentation-induced cracks was followed optically with a travelling microscope used to record linear dimensions. Section-and-etch techniques [9] were used to obtain cross-sectional profiles of the crack patterns in both glass and granite specimens *after* indenter removal. While the first of these procedures allows for a relatively rapid accumulation of fracture mechanics data,

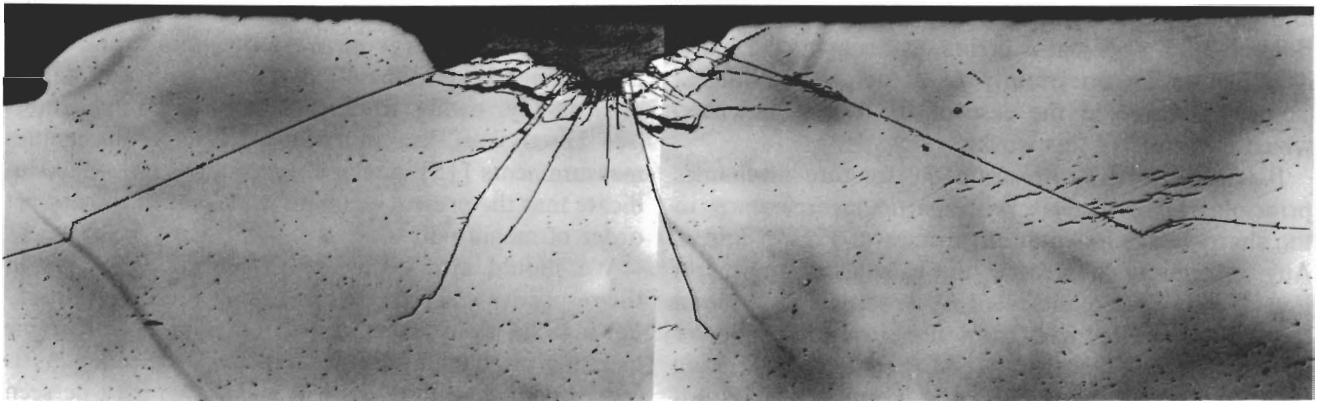
the second has the advantage of providing a ready means of comparing crack geometries in different materials: Figs. 5 and 6 accordingly illustrate cross-sectional profiles of indentation fracture patterns obtained in glass and granite specimens respectively, using wedge indenters.

Cracks formed during loading half-cycle

An extensive series of tests was carried out on soda-lime glass using the 'point' indenters of Fig. 4b, in an attempt to investigate the validity of Eq. (3b) for median and cone cracks. In these tests, sharp drops in the load-displacement curve were noted whenever a new crack suddenly overcame its formation energy barrier ('pop-in'). Due precaution against the recording of data not representative of configurations close to equilibrium was accordingly taken by continually translating the crosshair of the travelling microscope to predetermined positions ahead of the principal expanding crack, and by measuring the indenter load at the instant the crack tip reached each such position. The data obtained in this way have been reported in full elsewhere [6] and we confine our attention here to just 2 specific situations, those of median cracking under the action of sharp cone and wedge indenters. Figures 7 and 8 show the results, for several included half-angles in the case of cone indenters: the data points represent the experimental readings, and the

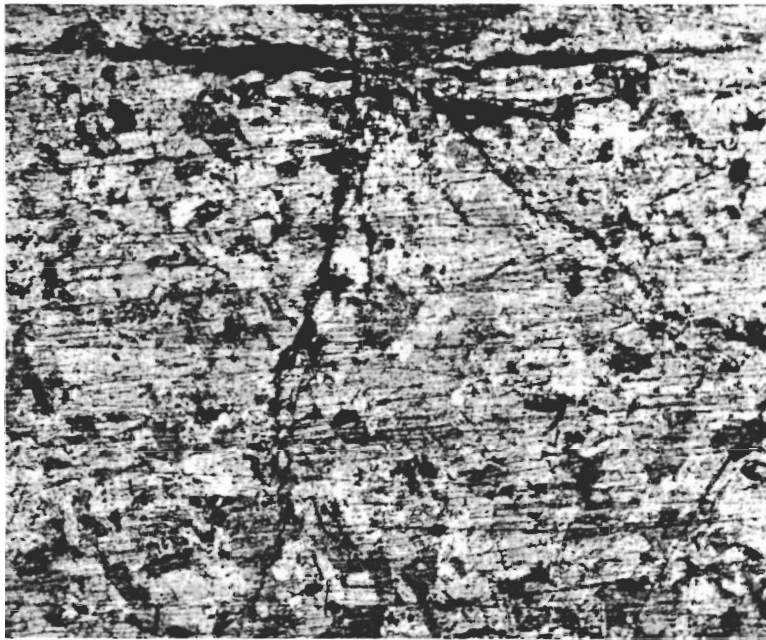


(a)

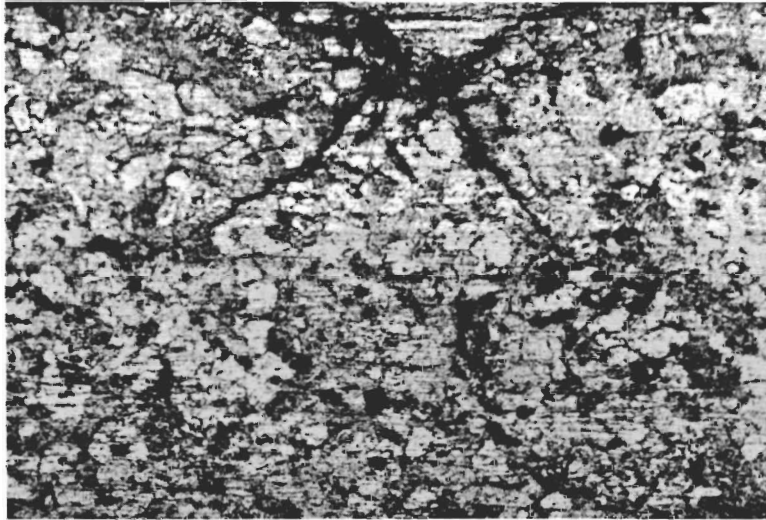


(b)

Fig. 5. Cross-section profiles of indentation fracture patterns in glass, in reflected light: (a) sharp wedge (Fig. 4a, left; $\psi = 37.5^\circ$, $P^m = 3.6$ kN); (b) blunt wedge (Fig. 4b, right; $P^m = 9.0$ kN). Width of field 18 mm. cf. Fig. 1.



(a)



(b)

Fig. 6. Cross-section profiles of indentation fracture patterns in granite, in reflected light: (a) sharp wedge (Fig. 4a, left; $\psi = 37.5^\circ$, $P^m = 5.9$ kN), (b) blunt wedge (Fig. 4b, right; $P^m = 16.2$ kN). Width of field 8 mm. cf. Figs. 1 and 5.

straight lines represent the theoretical predictions of Eqs. (3)–(5) for values $\Gamma = 3.9 \text{ Jm}^{-2}$, $E = 7.3 \times 10^{10} \text{ Pa}$ and $\nu = 0.25$ appropriate to soda–lime glass [13]. The random and systematic errors evident in the plots demonstrate an uncertainty of a factor of about 2 (somewhat more in the case of the wedge indenter) which is typical of this work.

It is of interest to illustrate the fracture mechanics principles involved here with particular reference to the sharp-wedge indentation profiles of Figs. 5 and 6. Any uncertainty inherent in the calculated κ terms of Eq. (4) may be circumvented by rewriting Eq. (3a) in the convenient reduced form (for invariant indenter geometry), $\Gamma_2/\Gamma_1 \approx (E_1/E_2)(P_{L2}/P_{L1})^2(c_1/c_2)$. Taking the measured value of Young's modulus $E = 3.4 \times 10^{10} \text{ Pa}$ for Westerly granite [14] in conjunction with the corresponding fracture parameters for

glass above, along with the comparative values of peak load and principal median crack length appropriate to Figs. 5a and 6a, we estimate Γ (granite) $\approx 30 \text{ Jm}^{-2}$. The fracture surface energy of Westerly granite (indeed of most minerals) is difficult to specify with any degree of accuracy, owing to microstructural complications (see Discussion), but independent fracture mechanics measurements [15], giving Γ (granite) $\approx 100 \text{ Jm}^{-2}$, indicate that the present estimate is at least of the correct order of magnitude.

We should also be aware of certain *differences* in the respective crack profiles of Figs. 5 and 6. In particular, a trend away from median cracking toward cone cracking in changing from sharp to blunt indenters is less evident in granite than in glass. This may be seen as a consequence of difference in mechanism of crack initiation. In granite, critical flaws develop more easily

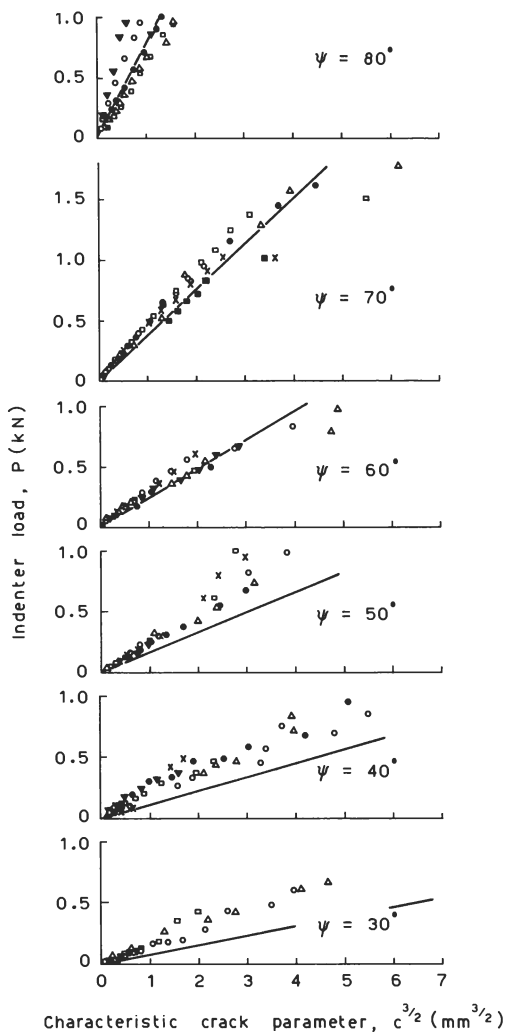


Fig. 7. Fracture mechanics relationships for median half-penny cracks in soda-lime glass, with WC conical indenters (half-angles as indicated). Data points represent experimental observations (each symbol a specific crack), full lines represent theoretical predictions.

directly below the indenter tip than in glass, presumably because of a greater microstructural weakness within the bulk.*

Cracks formed during unloading half-cycle

Very little attention has been paid to the mechanism of lateral cracking. Apart from the lack of an adequate theoretical description of this mode, experimental difficulties are evident. In particular, the degree of surface chipping observed under ostensibly invariant indentation loading conditions is found to vary considerably. This is seen in Fig. 9, obtained from soda-lime glass using the same sharp-cone indenters as those represented in Fig. 7. The data points in this figure correspond to the maximum dimension c' of the principal surface chip for a given peak load P^m , and the straight

*It is interesting to note that in relatively soft materials, such as glassy polymers, in quasi-static loading the median crack always tends to form before the cone crack, regardless of the geometry of the indenter [16]; in this instance the low level of stress at which flow processes operate prevents pre-existing surface flaws from becoming critical, and at the same time enhances deformation-induced fracture via a cumulative stress-concentration mechanism.

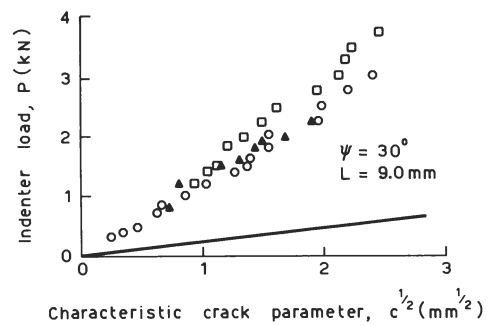


Fig. 8. Fracture mechanics relationship for median through cracks in soda-lime glass, with WC sharp wedge indenter (half-angle, wedge length as indicated). Data points represent experimental observations (each symbol a specific crack), full lines represent theoretical prediction.

lines are best-fit representations. Despite the wide scatter, it is clear that the linear scaling factor λ_p of Eq. (7b) is dependent on indenter geometry.

The comparative behaviour of glass and granite may be illustrated by further reference to the sharp-wedge indentation profiles of Figs. 5 and 6. We first rewrite Eq. (7b) in reduced form (invariant indenter geometry, scaling factor λ), $H_2/H_1 = (P_2^m/P_1^m) (c_1'^2/c_2'^2)$. From the appropriate values of peak load and lateral crack dimension in the figures, together with the typical value $H \approx 5.5 \times 10^9$ Pa for the hardness of silicate glass, we compute H (granite) $\approx 7.3 \times 10^9$ Pa. Independent measurements using a Vickers diamond pyramid (at $P^m = 100$ N) give H (granite) = $(4.9 \pm 0.3) \times 10^9$ Pa.

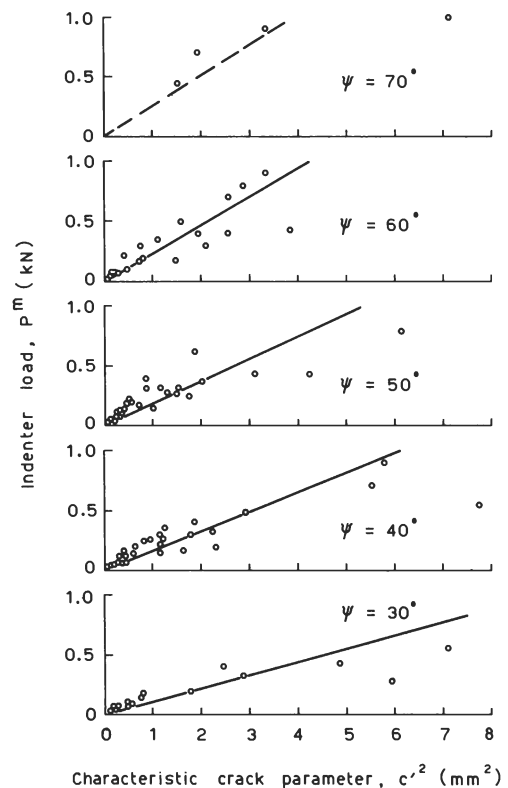


Fig. 9. Fracture mechanics relationships for lateral cracks in soda-lime glass, with WC conical indenters (half-angles as indicated). Data points represent experimental observations, full lines represent best-fit adjustments. Scarcity of data points at larger ψ reflects decreasing incidence of lateral crack intersection with specimen surface.

Again an uncertainty of a factor of about two is evident in the present work, consistent with the scatter shown in Fig. 9.

DISCUSSION

The comparative study of indentation damage in glass and granite described above provides compelling evidence for a tensile mode of failure in many geological fragmentation processes. More specifically, the study demonstrates the applicability of standard Griffith–Irwin fracture mechanics principles to the analysis of general indentation–crack configurations. This procedure represents a departure from the approach taken by several earlier workers. In the absence of direct observations of the evolution of cracking, as afforded in the present instance by comparison specimens of glass, there has been a tendency to associate indentation failure with a Coulomb–Mohr, ‘shear crack’ criterion [17–21]. Whereas such a criterion undoubtedly governs the failure of brittle materials in situations where hydrostatic compression completely suppresses any opening mode of crack propagation (i.e. at depth below the Earth’s surface), the same is not necessarily true for the general contact field in which the tensile component is by no means insignificant. Other workers, it is true, have acknowledged the possibility of tensile failure [22, 23], particularly in relation to the role of near-contact deformation (crushing, plasticity) in crack initiation. However, none have shown how the ultimate extent of cracking depends on the level of applied loading.

Our study, while far from complete in its treatment of many aspects of the problem (see below), does produce explicit relations for crack size in the limit of well-developed fracture. Moreover, these relations clearly identify the role of basic material parameters, such as fracture surface energy Γ and hardness H , in the overall crack propagation process. In this context it is interesting to note that variations in the microstructure of a given mineral can have a profound influence on both Γ (see for example, chapter 6 of Ref. [2]) and H [24], hence on the characteristic crack dimensions c and c' in Eqs. (3) and (7), respectively. Insofar as it is the lateral cracking Eq. (7) which is expected to figure more strongly in any detailed discussion of surface removal, these conclusions are not inconsistent with the thesis of the Westwood school that many rock fragmentation processes are largely hardness-controlled [25].

It is as well to be aware of some of the limitations inherent in the present analysis. For a start, we have focussed our attention on well-developed indentation fracture configurations. In the earlier stages of loading the scale of cracking relative to the scale of irreversible deformation about sharp indenter tips may be negligibly small, in which case surface removal may occur other than by brittle fracture [26]. Again, it has been assumed that equilibrium conditions prevail throughout, whereas in practical situations kinetic and dynamic effects can be important [3] (both Γ and H being

susceptible to environmental influences). Further, even for well-developed, equilibrium cracks, the fracture mechanics equations derived here are dependent upon somewhat ideal loading conditions: friction at the indenter/specimen interface [6, 22], and multiple evolution of cracks during any one indentation cycle [6], are just 2 factors which warrant further attention in this connection.

Much of previous rock testing has centred around the interpretation of force–displacement characteristics for complete indentation cycles. The scientific foundation for this type of test has been outlined by Gurney [27], who showed that the area enclosed by the characteristic curve associates closely with the area of new fracture surface created; in particular, in the special case of linear elastic materials loaded such that strain energy is lost only as work of stable crack propagation, the above areal quantities provide a direct measure of the fracture surface energy. This approach has been adopted by some workers [28] to determine fracture energies for certain brittle minerals. Generally, however, the indentation response is far from linear, with irreversible deformation about sharp indenter tips and sudden crack initiation events (accompanied by abrupt load drops in other than dead-weight loading devices) dissipating large proportions of the energy input. The usual way around such complications is to devise some alternative, empirical parameter, such as the volume of chipped material removed per unit of energy expenditure (the so-called ‘specific energy’) [21], to quantify the efficiency of the indentation cycle as a surface removal process. cursory investigations of the force–displacement curves for the glass and granite used in the present experiments indicate, among other things, that this efficiency can be improved by incorporating certain surfactants into the test environment [29]. We have already commented on the susceptibility of the basic fracture-controlling material parameters to extraneous influences.

Finally, mention may be made of the potential importance of *interactions* between individual indentation events in general surface removal phenomena. While lateral cracking clearly constitutes the most effective mode of chipping fracture, operating thus independently of neighbouring events, other cracking modes may contribute via an intersection mechanism as the density of events increases. Indeed, significant erosion of brittle surfaces may be realised under conditions in which lateral cracking does not occur at all [30]. The nature and relative importance of such interactions are complex issues in need of further study; to this end a recent semi-empirical fracture mechanics analysis of specific indentation crack interactions by Evans and Wilshaw [31] deserves special mention, particularly in regard to the role of fracture surface energy and hardness as controlling variables.

Acknowledgements—This work was supported in part by the Office of Naval Research (U.S.A.) under Contract No. NR-032-535 and in

part by the National Science Foundation (U.S.A.) under Grant GI38114. The assistance of E. R. Fuller and M. Rosenthal is gratefully acknowledged.

Received 19 January 1976.

REFERENCES

1. Kelly A. *Strong Solids*, Clarendon Press, Oxford (1966).
2. Lawn B. R. & Wilshaw T. R. *Fracture of Brittle Solids*, Cambridge University Press, Cambridge (1975).
3. Lawn B. R. & Wilshaw T. R. Indentation fracture: principles and applications. *J. Mat. Sci.* **10**, 1049–1081 (1975).
4. Lawn B. R. & Swain M. V. Microfracture beneath point indentations in brittle solids. *J. Mat. Sci.* **10**, 113–122 (1975).
5. Lawn B. R., Swain M. V. & Phillips K. On the mode of chipping fracture in brittle solids. *J. Mat. Sci.* **10**, 1236–1239 (1975).
6. Lawn B. R. & Fuller E. R. Equilibrium penny-like cracks in indentation fracture. *J. Mat. Sci.* **10**, 2016–2024 (1970).
7. Timoshenko S. & Goodier J. N. *Theory of Elasticity*, pp. 85–91, 362–366. McGraw-Hill, NY (1951).
8. Langitan F. B. & Lawn B. R. Effect of a reactive environment on the Hertzian strength of brittle solids. *J. appl. Phys.* **41**, 3357–3365 (1970).
9. Mikosza A. G. & Lawn B. R. Section-and-etch study of Hertzian fracture mechanics. *J. appl. Phys.* **42**, 5540–5545 (1971).
10. Frank F. C. & Lawn B. R. On the theory of Hertzian fracture. *Proc. R. Soc.* **1299**, 291–306 (1967).
11. Swain M. V., Williams J. S. & Lawn B. R. Cone crack closure in brittle solids. *Phys. Stat. Sol. (a)* **2**, 7–29 (1970).
12. Finnie I. & Vaidyanathan S. Initiation and propagation of Hertzian ring cracks. *Proc. Conf. Fracture Mechanics of Ceramics*, (Edited by R. C. Bradt, D. P. H. Hasselman & F. F. Lange), Vol. 1, pp. 231–244. Plenum Press, NY (1974).
13. Wiederhorn S. M. Fracture surface energy of glass. *J. Am. Ceram. Soc.* **52**, 99–105 (1969).
14. Simmons G. & Brace W. F. Comparison of static and dynamic measurements of compressibility of rocks. *J. Geophys. Res.* **70**, 5649–5646 (1965).
15. Hoagland R. G., Hahn G. T. & Rosenfield A. R. Influence of microstructure on fracture propagation in rocks. Semiannual Research Report, Batelle Columbus Laboratories, ARPA Contract No. H0210006 (1971).
16. Puttick K. E., Miller L. E. & Gillham E. Stress fields around indentations in polymethylmethacrylate, to be published.
17. Cheatham J. B. An analytical study of rock penetration by a single bit tooth. *Proc. 8th Drilling and Blasting Symp., Minnesota*, pp. 1A–24A. Pergamon, NY (1958).
18. Paul B. & Sikarskie D. L. A preliminary model for wedge penetration in brittle materials. *Trans. Am. Inst. Min. Engrs.* **232**, 372–383 (1965).
19. Dutta P. K. A theory of percussive drill bit penetration. *Int. J. Rock Mech. Min. Sci.* **9**, 543–567 (1972).
20. Lundberg B. Penetration of rock by conical indenters. *Int. J. Rock Mech. Min. Sci. & Geomech. Abstr.* **11**, 209–214 (1974).
21. Paone J. & Tandanand S. Inelastic deformation of rock under a hemispherical drill bit. *Trans. Am. Inst. Min. Engrs.* **235**, 113–123 (1966).
22. Reichmuth D. R. Correlation of force–displacement data with physical properties of rock for percussive drilling systems. *Proc. 5th Symp. Rock Mechanics, Minnesota*, pp. 33–59. Pergamon, NY (1963).
23. Graham J. Damage induced by a sliding diamond—an approach to hard rock drilling. *Rock Mech.* **4**, 191–202 (1972).
24. Rice R. W. Correlation of hardness with mechanical effects in ceramics. *Proc. Conf. on The Science of Hardness Testing and its Research Applications*, (Edited by J. H. Westbrook & H. Conrad), pp. 117–134. American Society for Metals, Metals Park, OH (1971).
25. Westwood A. R. C. Control and application of environment-sensitive fracture processes. *J. Mat. Sci.* **9**, 1871–1895 (1974).
26. Lawn B. R., Jensen T. & Arora A. Brittleness as an indentation size effect. *J. Mat. Sci.* **11**, 573–575 (1976).
27. Gurney C., Mai Y. W. & Owen R. C. Quasistatic cracking of materials with high fracture toughness and low yield stress. *Proc. R. Soc.* **A340**, 213–231 (1974).
28. Friedman M., Handin J. & Alani G. Fracture-surface energy of rocks. *Int. J. Rock Mech. Min. Sci.* **9**, 757–766 (1972).
29. Swain M. V. Unpublished work.
30. Adler W. F. Analysis of multiple particle impacts on brittle materials. Technical Report AFML-TR-74-210, Textron's Bell Aerospace Co. (1974).
31. Evans A. G. & Wilshaw T. R. Quasistatic solid particle damage in brittle solids—I. Observations and analysis. Technical Report SC5023.3TR, Rockwell International Science Center (1975).